

Article

# Advanced Electrodegradation of Doxorubicin in Water Using a 3-D Ti/SnO<sub>2</sub> Anode

Corina Orha <sup>1</sup>, Cornelia Bandas <sup>1</sup>, Carmen Lazau <sup>1</sup>, Mina Ionela Popescu <sup>1</sup>, Anamaria Baciu <sup>2</sup> and Florica Manea <sup>2,\*</sup>

- <sup>1</sup> Condensed Matter Department, National Institute for Research and Development in Electrochemistry and Condensed Matter, Timisoara, 1 Plautius Andronescu Street, 300254 Timisoara, Romania; orha.corina@gmail.com (C.O.); cornelia.bandas@gmail.com (C.B.); carmen.lazau@gmail.com (C.L.); mina.popescu37@gmail.com (M.I.P.)
- <sup>2</sup> Department of Applied Chemistry and Engineering of Inorganic Compounds and Environment, Politehnica University of Timisoara, Blv. Vasile Parvan No. 6, 300223 Timisoara, Romania; anamaria.baciu@upt.ro
- \* Correspondence: florica.manea@upt.ro

**Abstract:** This study investigated the application of an advanced electrooxidation process with three-dimensional tin oxide deposited onto a titanium plate anode, named 3-D Ti/SnO<sub>2</sub>, for the degradation and mineralization of one of the most important emerging contaminants with cytostatic properties, doxorubicin (DOX). The anode was synthesized using a commercial Ti plate, with corrosion control in acidic medium, used as a substrate for SnO<sub>2</sub> deposition by the spin-coating method. X-ray diffraction (XRD) and scanning electron microscopy (SEM) analyses revealed that porous SnO<sub>2</sub> was obtained, and the rutile phase of TiO<sub>2</sub> was identified as an intermediary substrate onto the Ti plate. The results of CV analysis allowed us to determine the optimal operating conditions for the electrooxidation process conducted under a constant potential regime, controlled by the electron transfer or the diffusion mechanisms, involving hydroxyl radicals. The determination of UV-VIS spectra, total organic carbon (TOC), and chemical oxygen demand (COD) allowed us to identify the degradation mechanism and pathway of DOX onto the 3-D Ti/SnO<sub>2</sub> anode. The effective degradation and mineralization of DOX contained in water by the electrooxidation process with this new 3-D dimensionally stable anode (DSA) was demonstrated in this study.

**Keywords:** doxorubicin; emerging pollutants in water; advanced water treatment; advanced electrooxidation; porous dimensionally stable anode (DSA); Ti/SnO<sub>2</sub>



**Citation:** Orha, C.; Bandas, C.; Lazau, C.; Popescu, M.I.; Baciu, A.; Manea, F. Advanced Electrodegradation of Doxorubicin in Water Using a 3-D Ti/SnO<sub>2</sub> Anode. *Water* **2022**, *14*, 821. <https://doi.org/10.3390/w14050821>

Academic Editor: Christos S. Akkratos

Received: 3 February 2022

Accepted: 3 March 2022

Published: 6 March 2022

**Publisher's Note:** MDPI stays neutral with regard to jurisdictional claims in published maps and institutional affiliations.



**Copyright:** © 2022 by the authors. Licensee MDPI, Basel, Switzerland. This article is an open access article distributed under the terms and conditions of the Creative Commons Attribution (CC BY) license (<https://creativecommons.org/licenses/by/4.0/>).

## 1. Introduction

Pharmaceutically active compounds (PhACs) are included into the category of emerging pollutants present in water, and their presence has been reported in every aqueous ecosystem. The main source of pharmaceuticals is represented by wastewaters from hospitals, manufacturing aquaculture facilities, and landfill leachate, which are in generally discharged into municipal wastewater treatment plants (WWTP). The conventional WWTP technology is not able to completely remove pharmaceuticals, and thus, WWTP effluents act as major sources of discharges of various mixtures of pharmaceuticals into the environment [1,2]. Considering that cancer is one of the most serious diseases diffused in the world, it is obviously that the consumption of cytostatics is increasing and, as consequence, their presence in the environment will continue to rise [3]. Because of their carcinogenic, mutagenic, and teratogenic properties, cytostatics have a very negative environmental impact, especially on water, and as consequence, pose serious risks to human health [4]. Doxorubicin (DOX) is an anthracycline antibiotic used frequently to treat cancer via DNA intercalation. It consists of the tetracyclic quinoid aglycone adriamycinone (14-hydroxydaunomycinone) linked to the amino sugar daunosamine [5].

Electrooxidation processes are an alternative to the conventional water/wastewater treatment and can be easily integrated within and improve the current treatment technologies, thanks to their main useful features, i.e., versatility, environmental compatibility, facility of automation, potential cost effectiveness, and safety in relation to their mild operating conditions [6,7].

There are several reports regarding the application of electrooxidation processes for the degradation/mineralization of pharmaceuticals as emerging pollutants from water [8–11], including cytostatic removal from water [6,7]. However, few studies have been reported on the electrooxidation of DOX [7,12].

The anode material represents the core aspect responsible for the process efficiency, which depends on the electrode performance in the degradation/mineralization process of pharmaceuticals contained in water. The electrode function is influenced by the operating conditions and the water content of chloride as a precursor of chlorine, which should improve the electro degradation/mineralization degree. The most studied and efficient anode materials applied in advanced electrooxidation processes that assure pharmaceuticals' mineralization are the boron-doped diamond electrode (BDD) and dimensionally stable anodes (DSAs) [13–15].

The BDD anode is a non-active electrode material, while DSAs can be non-active or active in the advanced electrooxidation process in relation to their composition, on the basis of the classification proposed by Comninelis [16]. Active DSAs are characterized by a low over potential for the oxygen evolution reaction (OER) and a strong interaction with electrogenerated hydroxyl radicals, while non-active electrodes (e.g.,  $\text{SnO}_2$ ) exhibit a high over potential for OER, which makes them appropriate for processes based on indirect oxidation [17,18].

In general, DSAs are a very promising class of the electrode materials in advanced electrooxidation processes due to the fact that they are dimensionally stable and good conductors, exhibit high catalytic activity, and contribute towards energy saving [19]. The synthesis method of DSA influences their features. There are many preparation methods of DSA electrodes, including the sol-gel technique [20,21], electrodeposition [22,23], chemical vapor decomposition [24], dip-coating [25], the hydrothermal method [26], sputtering [27], ultrasonic atomization decomposition [28,29], and self-assembly method [30,31].

The chemical and physical properties of the anode depend on the size and shape of its particles, in addition to its composition. It is well known that the preparation conditions, e.g., the structure-directing agent, the nature of the precursor, and the sintering temperatures, affect the physical properties and stability of electrodes. The morpho-structural characteristics of DSAs related to their porosity allow designing the anode configuration as two-dimensional (2-D) for a low porosity of the electrode surface and as three-dimensional (3-D) for a high porosity of the electrode surface. Porous DSAs have a longer lifetime in comparison with DSAs with a smoother surface and also a larger specific active area and a higher overpotential for OER, which improves the electrochemical activity in advanced degradation/mineralization processes [32].

In this work, a porous 3-D DSA consisting of  $\text{SnO}_2$  deposited onto a corroded Ti plate, named Ti/ $\text{SnO}_2$  electrode, was synthesized by the spin-coating method and tested in the advanced degradation/mineralization of the cytostatic pharmaceutical doxorubicin (DOX), an emerging water pollutant. The Ti/ $\text{SnO}_2$  electrode was characterized morpho-structurally and electrochemically and tested in the advanced electro degradation/mineralization of DOX from water in the presence/absence of chloride. The operating conditions for DOX electrooxidation were optimized using the chronoamperometry technique (CA) that simulates a potentiostatic regime operation to achieve the best mineralization performance. UV-VIS spectra, Chemical Oxygen Demand (COD), and TOC parameters were analyzed to elucidate several aspects related to the degradation mechanism of DOX using the Ti/ $\text{SnO}_2$  electrode.

## 2. Materials and Methods

### 2.1. Preparation of the DSA Electrode

Preparation of the Ti/SnO<sub>2</sub> electrode in three stages:

1. *Pretreatment of a titanium plate's surface:* First, a titanium plate (1 × 1 cm) was sanded with sandpaper P4000, followed by an ultrasonic treatment in deionized water for 30 min. Then, it was placed in a 10% (wt%) sodium hydroxide solution for 1 h at 80 °C and finally in a 10% (wt%) oxalic acid solution, for 2 h at 80 °C. Lastly, the Ti substrate were rinsed sequentially with acetone, ethanol, and deionized water and the dried at 60 °C.
2. *Preparation of an SnO<sub>2</sub> gel:* Anhydrous tin chloride (SnCl<sub>2</sub>, 99%, Aldrich) was used as a tin source, and polyethylene glycol Pluronic P-123 (Aldrich) was applied as the structure-directing agent. All chemicals were used without further purification. SnO<sub>2</sub> samples were synthesized using a sol-gel method as follows: a solution was prepared by dispersing 1.5 g of Pluronic P-123 in 15 mL ethanol over 1 h at 40 °C. Then, the solution was mixed with 5 mL of SnCl<sub>2</sub> and 10 mL of distilled water under continuous stirring. An appropriate amount of HCl was then added to adjust the acidity of the solution. After 4 h of mixing, the transparent gel was left standing to age for 3 weeks in a hermetic dark recipient.
3. *Preparation of the Ti/SnO<sub>2</sub> electrode:* The Ti/SnO<sub>2</sub> electrode was obtained by the spin-coating method (WS-400-6NPPB Spin Coater-Laurell Technology Corporation) by deposition of SnO<sub>2</sub> thin films on Ti plates, according to following protocol: 0.1 g of SnO<sub>2</sub> transparent gel was diluted with 1 mL of ethanol and subjected to ultrasound for 20 min. Then, 100 µL of gel was deposited under rotation at 3000 rot/min for 10 s and subsequently dried for 30 min at 60 °C. After repeating this process 6 times, the samples were calcined at 500 °C for 1 h at a ramping rate of 1 °C/min to ensure the complete decomposition of the organic polymer and improve the crystallinity of the particles.

### 2.2. Characterization of the DSA Electrode

The morpho-structural properties of the porous Ti/SnO<sub>2</sub> were characterized by scanning electron microscopy coupled with energy-dispersive X-ray (SEM/EDX, Inspect S model, Eindhoven, The Netherlands) and X-ray diffraction (XRD PANalytical X'Pert PRO MPD Diffractometer, Almelo, The Netherlands).

The electrochemical characterization of the Ti/SnO<sub>2</sub> electrode was performed by cyclic voltammetry with a classical three-electrode cell system, consisting of a working electrode, a platinum counter electrode, and a saturated calomel reference electrode using an Autolab potentiostat/galvanostat PGSTAT 302 (Eco Chemie, Utrecht, The Netherlands) controlled with GPES 4.9 software.

### 2.3. Testing the DSA Electrode for DOX Degradation

Electrochemical degradation and mineralization were conducted under potentiostatic regime through chronoamperometry using the same above-presented three-electrode cell system, which allowed the assessment of the electrode material for DOX degradation and mineralization.

DOX belongs to the anthracyclines group, characterized by a tetracycline ring structure with a daunosamine group (a sugar moiety). It is a derivate of anthraquinone, composed of aglycone (4 rings connected to each other—A, B, C, D) and the sugar moiety attached by a glycosidic linkage at the C-7 position of the A-ring [33,34].

The spectral profile of DOX is very complex mainly because of the presence of absorption bands corresponding to benzenoid transitions besides the quinonoid absorption bands. In accordance with the literature, the peak maxima at about 253 and 290 were assigned to a  $\pi$ - $\pi^*$  transition of the aromatic ring (benzenoid band) and the quinonoid structure [33,34]; the presence of the dioxyderivative substituents led to absorption maxima at 486 nm [35,36].

The absorption band at 232 nm was assigned to the n- $\sigma^*$  transition of the methoxy group of DOX [37].

Based on the absorbance peaks in the UV-VIS spectra of DOX (Figure 1), the electrochemical degradation process was assessed by both the degree of color removal based on the absorbance recorded at 486 nm ( $A_{486}$ ) and the degradation degree determined through the absorbances recorded at 232 nm ( $A_{232}$ ), 253 nm ( $A_{253}$ ), and 290 nm ( $A_{290}$ ).

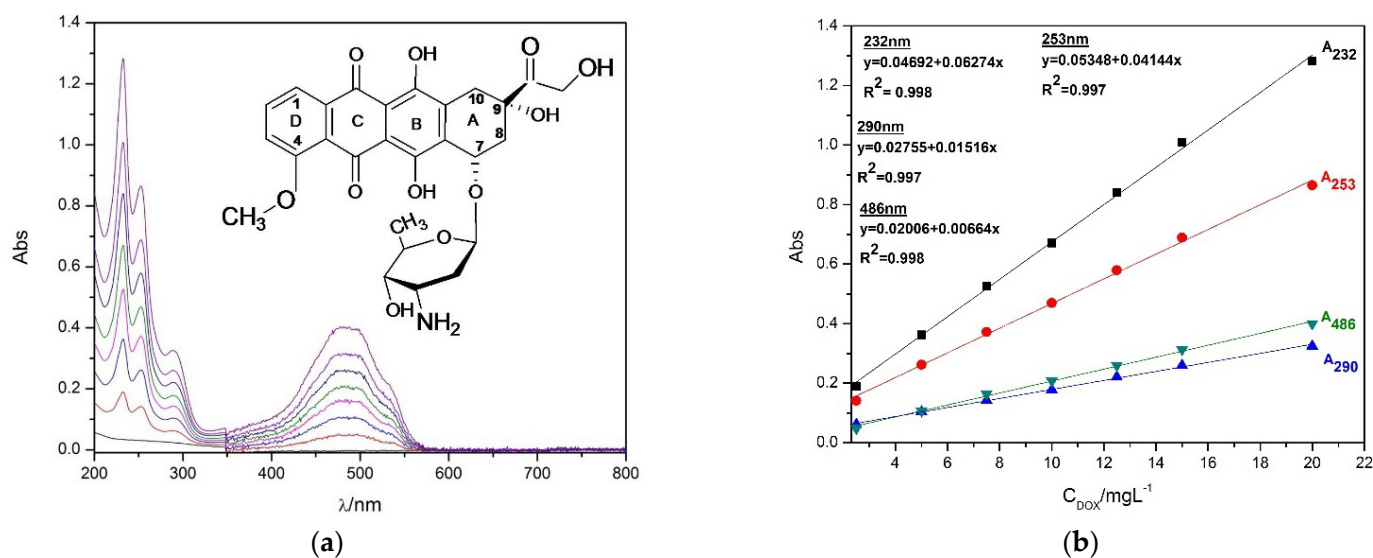


**Figure 1.** UV-VIS spectra for different concentration of DOX (2.5; 5; 7.5; 10; 12.5; 15; 20 mg·L<sup>-1</sup>) (a); linear calibration curves of maximum peak absorbances vs. DOX concentrations (b).

The DOX degradation degree ( $\eta$ ) and electrochemical degradation degree ( $E_{DOX}$ ) were determined based on Equations (1) and (2):

$$\eta = \frac{(C_{DOX,i} - C_{DOX,f})}{C_{DOX,i}} \cdot 100(\%) \quad (1)$$

$$E = \frac{(C_{DOX,i} - C_{DOX,f})}{C \cdot S} \cdot V(\text{mg}/\text{C} \cdot \text{cm}^2) \quad (2)$$

where  $C_{DOX,i} - C_{DOX,f}$  represents the change in DOX concentration, determined by spectrophotometry at each absorbance (486 nm, 290 nm, 253 nm, and 232 nm), during the electrochemical experiments for a charge consumption of  $C$  corresponding to various electrolysis times,  $V$  is the sample volume (20 cm<sup>3</sup>), and  $S$  is the area of the electrode surface (0.64 cm<sup>2</sup>).

The electrochemical mineralization degree ( $E_{TOC}$ ) was also evaluated for optimum operating conditions, considering the change in  $TOC$  concentration instead of DOX concentration, based on Equation (3):

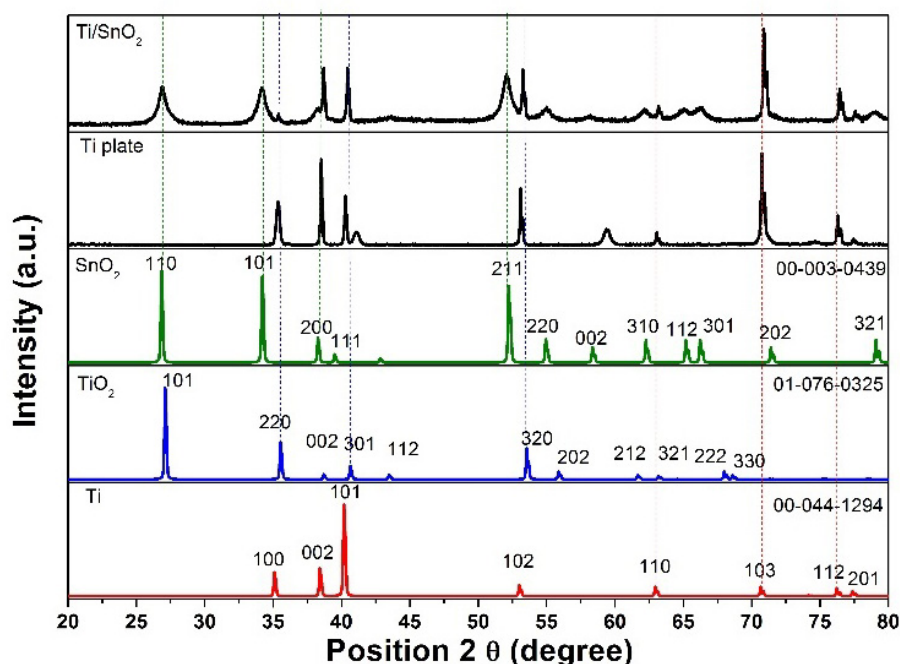
$$E_{TOC} = \frac{(TOC_i - TOC_f)}{C \cdot S} \cdot V(\text{mg}/\text{C} \cdot \text{cm}^2) \quad (3)$$

The chemical oxygen demand (COD) was determined according to standard methods [38], and total organic carbon (TOC) was analyzed by a Shimadzu TOC analyzer (Columbia, MD, USA).

### 3. Results and Discussion

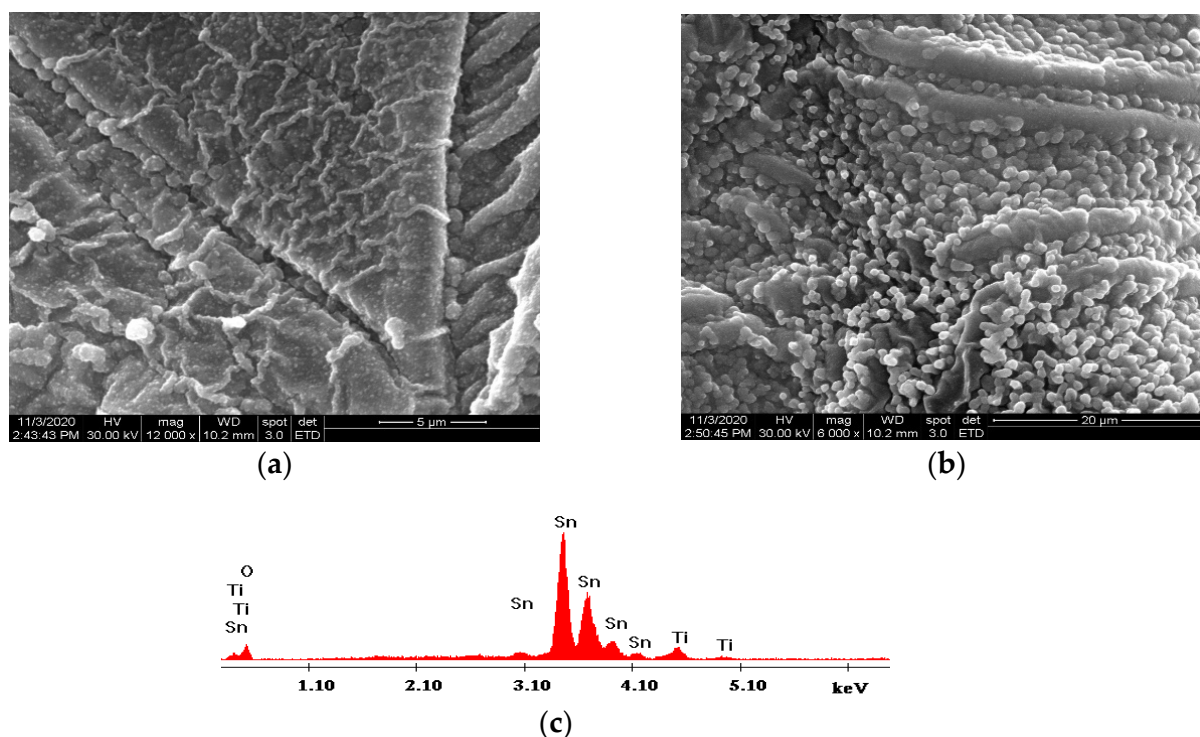
#### 3.1. Morpho-Structural Characterization of Ti/SnO<sub>2</sub>

Figure 2 presents the XRD spectrum of the Ti/SnO<sub>2</sub> electrode in comparison with those of Ti, TiO<sub>2</sub> and SnO<sub>2</sub>. The peaks (100), (002), (101), (102), (110), (103) (112) of the corroded Ti plate are in accordance with the database card no. 00-044-1294 for Ti; the rutile phase of TiO<sub>2</sub> due to the thermal treatment at 500°C was identified by peaks (101), (220), (301), (320) based on the JCPDS 01-076-0325 databases. The presence of the rutile phase of TiO<sub>2</sub> was due to the partial oxidation of the Ti plate under acidic conditions during the corrosion process used to enlarge the Ti plate porosity. The peaks (110), (101), (200), (211) noticed at 2θ: 26.57; 33.89; 38.42; 52.5 indicated a well-crystallized SnO<sub>2</sub>.



**Figure 2.** XRD spectrum of the Ti/SnO<sub>2</sub> electrode surface in comparison with those of Ti, TiO<sub>2</sub>, and SnO<sub>2</sub>.

Figure 3 shows the SEM images and EDX spectrum of a Ti/SnO<sub>2</sub> electrode prepared through the deposition of six layers, which indicate that the SnO<sub>2</sub> film surface was homogenous, with a compact texture without holes. The results indicate that the spherical mesoporous and microstructural nature of the SnO<sub>2</sub> films was obtained from the optimized tin gel deposited onto the corroded Ti plate. For comparison, this gel was deposited onto a non-corroded Ti plate, and the classical 2-D smooth and compact morphology containing mud-like cracks was observed (results not shown), which proved that Ti corrosion in an acidic medium assured obtaining a 3-D Ti/SnO<sub>2</sub> electrode with a mesoporous surface. In addition, EDX analysis (Figure 3c) coupled with SEM confirmed that the electrode surface consisted of tin and oxygen elements, indicating that pure SnO<sub>2</sub> microparticles were deposited onto the partial oxidized Ti plate, in accordance with the X-ray results presented in Figure 2.



**Figure 3.** SEM images of the Ti/SnO<sub>2</sub> electrode at different magnifications: (a) 12,000 $\times$ ; (b) 6000 $\times$ ; (c) EDX image of the Ti/SnO<sub>2</sub> electrode.

### 3.2. Electrochemical Characterization through CV

The cyclic voltammograms recorded on Ti/SnO<sub>2</sub> in the supporting electrolytes 0.1 M Na<sub>2</sub>SO<sub>4</sub> and 0.05 M Na<sub>2</sub>SO<sub>4</sub> plus 0.05 M NaCl, in the absence/presence of 5 mg·L<sup>-1</sup> of DOX within the potential range between -1.00 and +4.00 V/SCE are presented in Figure 4. A high overpotential of about +2.50 V/SCE for OER was noticed in 0.1 M Na<sub>2</sub>SO<sub>4</sub> supporting electrolyte, which is characteristic of a non-active anode and is in accordance with the literature [39]. The presence of 5 mg·L<sup>-1</sup> of DOX exerted a light polarization effect on the OER, which was also manifested by the chloride presence in the supporting electrolyte.

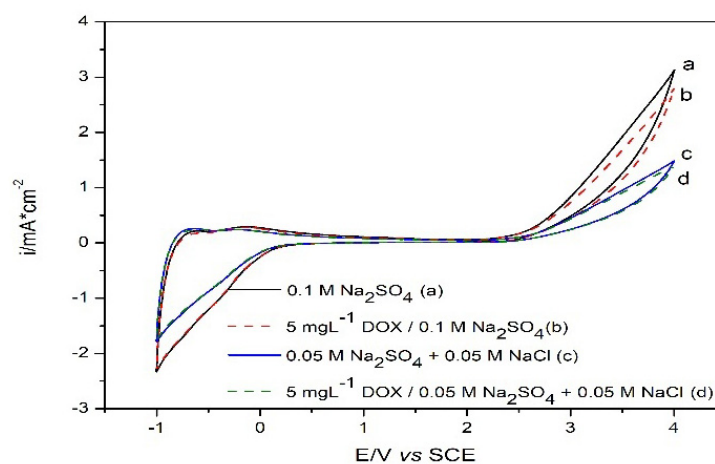


**Figure 4.** Cyclic voltammograms recorded at the Ti/SnO<sub>2</sub> electrode in the absence and the presence of 5.00 mg·L<sup>-1</sup> of DOX between -1.00 and +4.00 V vs. SCE in 0.1 M Na<sub>2</sub>SO<sub>4</sub> supporting electrolyte (a, b) and 0.05 M Na<sub>2</sub>SO<sub>4</sub> + 0.05 M NaCl supporting electrolyte (c, d).

The determination of the starting overpotential for the OER is very important as it allows conducting the degradation test under potential conditions of OER generating hydroxyl radicals, according to the Equation (4):



Considering the composition of the aqueous supporting electrolyte, within the anodic process, ozone, chlorine, and persulphate were generated, besides hydroxyl radicals, based on reactions (5–8); these molecules could act as oxidizing agents during the electrolysis.



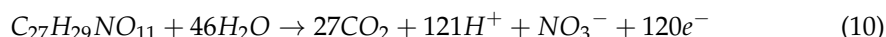
### 3.3. Testing Ti/SnO<sub>2</sub> in DOX Degradation and Mineralization

The electrochemical degradation/mineralization of DOX was carried out in the potentiostatic regime through chronoamperometry at two potential values, +3.00 V vs. SCE and +4.00 V vs. SCE, which were selected based on the CV results considering the oxygen evolution reaction. It is known that the electrode reaction is controlled either by the electrical charge transfer or by the mass transfer of the electroactive species from the bulk of the solution to the electrode, depending on the applied current density or corresponding overpotential. When the applied current density is higher than the limiting current density ( $i_{lim}$ ), the process is controlled by diffusion, and when the applied current density is lower than  $i_{lim}$ , the process is controlled by electrical charge transfer.  $i_{lim}$  (A/m<sup>2</sup>) can be calculated according to Equation (9) used for similar studies [9,40]:

$$i_{lim} = zFDC_{DOX} \quad (9)$$

where  $i_{lim}$  is the limiting current density for DOX mineralization (A·m<sup>-2</sup>),  $z$  is the number of electrons involved in the organic mineralization reaction (9),  $F$  is the Faraday constant 96,487 C·mol<sup>-1</sup>,  $D$  is the mass transfer (diffusion) coefficient (m<sup>2</sup>·s<sup>-1</sup>), and  $C_{DOX}$  is DOX concentration in the bulk solution (mol·m<sup>-3</sup>).

The mineralization reaction of DOX was considered to be based on the Equation (10):



Taking into account the conditions for O<sub>2</sub>, O<sub>3</sub>, hydroxyl radicals, and Cl<sub>2</sub> generation, according to the reactions (4–8), the electrode performance in the oxidation process was assessed comparatively in both 0.1 M Na<sub>2</sub>SO<sub>4</sub> and 0.05 M Na<sub>2</sub>SO<sub>4</sub> + 0.05 M NaCl supporting electrolytes. Figure 5 shows the chronoamperometric results selected as examples for the potential of +4.00 V/SCE, in the presence of various DOX concentrations and comparing the two supporting electrolytes.

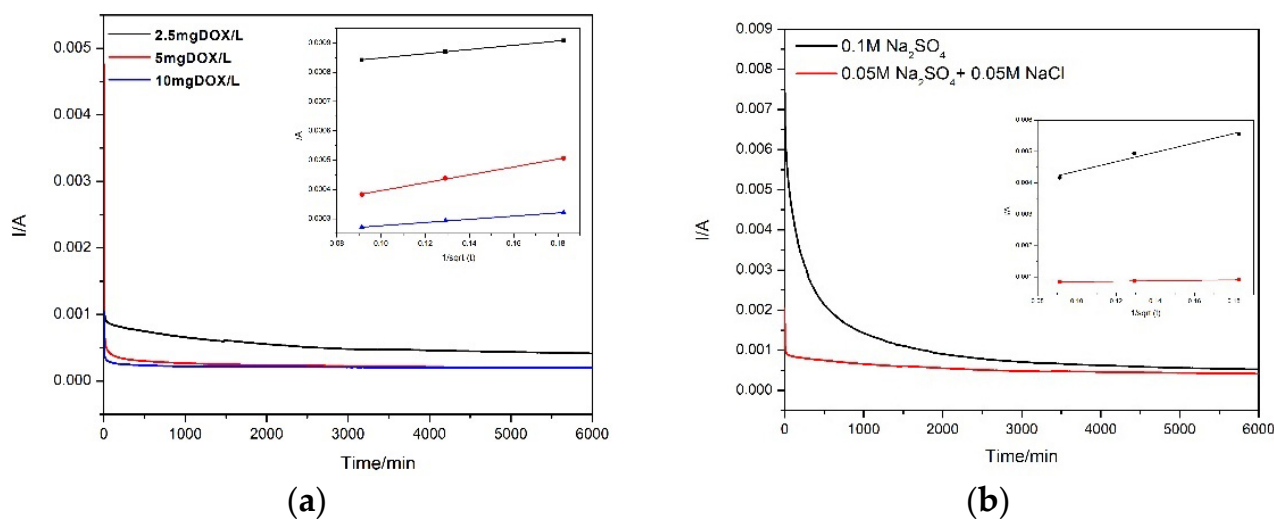


**Figure 5.** Chronoamperograms recorded with the Ti/SnO<sub>2</sub> electrode at a potential of +4.00 V in: (a) 0.05 M Na<sub>2</sub>SO<sub>4</sub> +0.05 M NaCl supporting electrolyte and 2.5, 5, and 10 mg·L<sup>-1</sup> DOX; Inset: linearization of the Cottrell equation; (b) 2.5 mg·L<sup>-1</sup> DOX and supporting electrolyte consisting of 0.05 M Na<sub>2</sub>SO<sub>4</sub> +0.05 M NaCl and 0.1 M Na<sub>2</sub>SO<sub>4</sub>; Inset: linearization of the Cottrell equation.

The chronoamperometric results recorded at +4.00 V/SCE allowed determining the diffusion coefficient of DOX in the tested conditions, based on the Cottrell equation [9,41]:

$$I(t) = nFAC^* \left( \frac{D}{\pi t} \right)^{1/2} \quad (11)$$

where  $D$  represent the diffusion coefficient ( $\text{cm}^2 \cdot \text{s}^{-1}$ ), and  $C^*$  is the concentration of the target solution ( $\text{mol} \cdot \text{cm}^{-3}$ ). Based on the linear dependence between  $I$  and  $t^{-1/2}$  in as short time (30 min), the diffusion coefficient can be determined from the slope given by the term  $nFAC^*(D/\pi)^{1/2}$ . The calculated diffusion constants are presented in Table 1. It can be noticed that DOX diffusion constant depended on the supporting electrolyte. The presence of  $\text{Cl}^-$  did not improve the diffusion constant, probably due to other secondary reactions involving chlorine and hypochlorite generation (Equations (5) and (6)), which acted as oxidants for DOX degradation. At a higher concentration, DOX diffusion to the electrode surface slightly decreased, probably due to its accumulation on the electrode surface.

**Table 1.** Diffusion constant determined by the slope of the Cottrell equation for CA operated at +4.00 V/SCE.

Supporting Electrolyte	DOX Concentration/ mg·L <sup>-1</sup>	Diffusion Constant, $D \cdot 10^9$ ( $\text{cm}^2 \cdot \text{s}^{-1}$ )
0.05 M Na <sub>2</sub> SO <sub>4</sub> + 0.05 M NaCl	2.5	1.40
	5	1.23
	10	0.60
0.1 M Na <sub>2</sub> SO <sub>4</sub>	2.5	5.70

The assessment of the electrochemical degradation and mineralization of DOX using Ti/SnO<sub>2</sub> was carried out based on the DOX degradation degree and the electrochemical degradation efficiency using Equations (1) and (2), considering the peak maximum recorded at each wavelength and TOC. Figure 6 shows the degradation degrees achieved by applying two values of potential, i.e., +3.00 and +4.00 V/SCE in 0.1 M Na<sub>2</sub>SO<sub>4</sub> supporting electrolyte. It is obvious that the DOX degradation degree was much higher at +4.00 V/SCE than at +3.00 V/SCE. The largest difference was found for the color removal degree assessed

by the absorbance recorded at 486 nm, which was seven times higher at +4.00 V/SCE than at +3.00 V/SCE, due to the higher concentration of hydroxyls that easily attacked the chromophore groups of DOX.

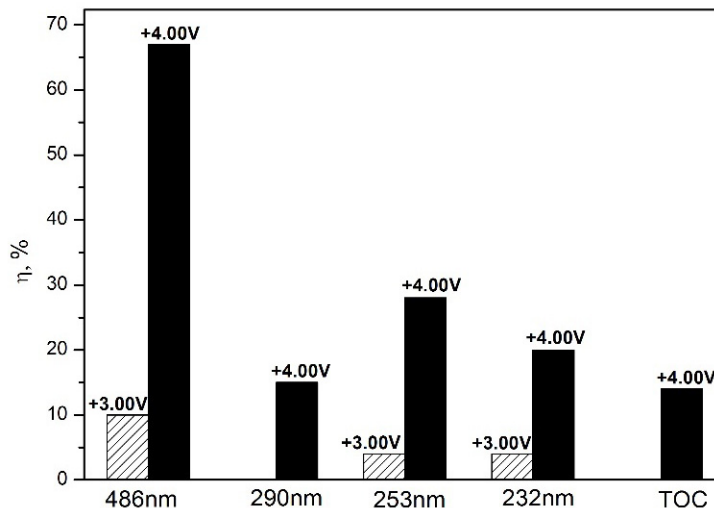


**Figure 6.** DOX degradation degree after 2 h of chronoamperometry running at +3.00 V/SCE and +4.00 V/SCE in 0.1 M Na<sub>2</sub>SO<sub>4</sub> supporting electrolyte, with 2.5 mg · L<sup>-1</sup> DOX.

Under these conditions, electrochemical DOX conversion without mineralization at the potential of +3.00 V/ESC and a low mineralization degree (about 10%) for the potential value of +4.00 V/ESC were achieved.

The effect of the supporting electrolyte due to the presence of chloride was examined; the results are presented in Figure 7. As it is well known, chlorine and other chlorine-based species are generated in this electrode potential range, in agreement with reactions (6, 7) and act as oxidation agents in DOX degradation (besides hydroxyls radicals), improving the degradation and mineralization efficiency.

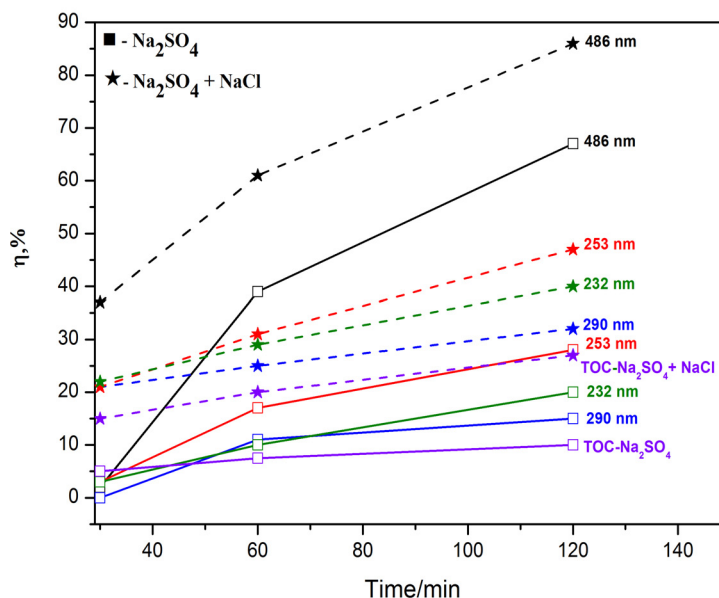


**Figure 7.** DOX degradation and mineralization degree after chronoamperometry at +4.00 V/SCE with 2.5 mg · L<sup>-1</sup> DOX, in 0.1 M Na<sub>2</sub>SO<sub>4</sub> supporting electrolyte (dots line) and in 0.05 M Na<sub>2</sub>SO<sub>4</sub> + 0.05 M NaCl supporting electrolyte (continuous line).

Based on UV–VIS spectra evolution during the electrooxidation process presented as degradation and mineralization degrees, for both supporting electrolytes, in the first stage of degradation, the color was removed due to the first attack of the hydroxyl radicals focused on the chromophore group attributed to the dioxyderivative substituents; then, the quinonoid structures were degraded, followed by the methoxy substituent. Finally, the aromatic rings were broken. The superiority of the DOX degradation process efficiency performed in the presence of chloride was easily proved by the UV–VIS spectra recorded before and after DOX electrooxidation in both supporting electrolytes (Figure 8).

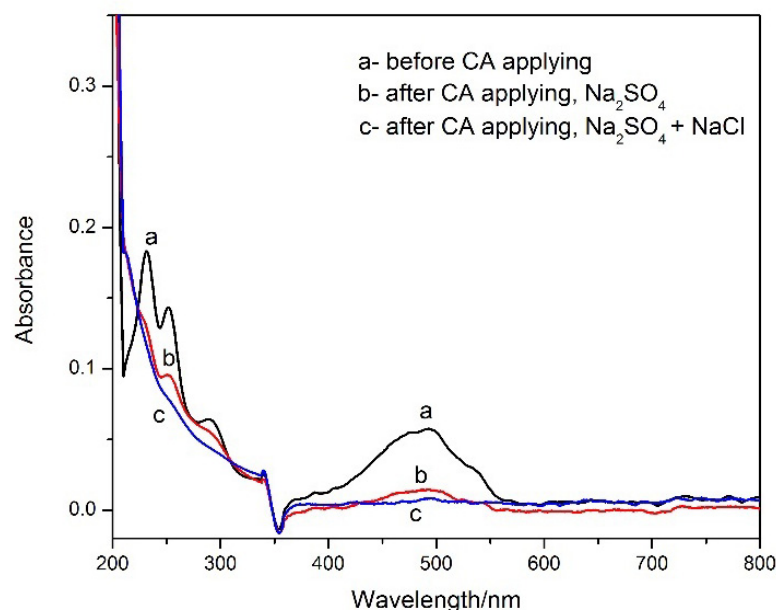


**Figure 8.** UV–VIS spectra recorded for  $2.5 \text{ mg}\cdot\text{L}^{-1}$  DOX before (curve a) and after electrooxidation by CA operated at  $+4.00 \text{ V/SCE}$  in the supporting electrolytes  $0.1 \text{ M Na}_2\text{SO}_4$  (curve b) and  $0.05 \text{ M Na}_2\text{SO}_4 + 0.05 \text{ M NaCl}$  (curve c).

To assess the electrochemical performance of the electrode and process, electrical charge consumption during the electrooxidation was taken into account and expressed as the degree of electrochemical degradation and mineralization, in agreement with Equations (2) and (3). Based on Equations (9) and (11), for  $2.50 \text{ mg}\cdot\text{L}^{-1}$  DOX,  $i_{\text{lim}} = 13.0 \text{ A}\cdot\text{m}^{-2}$  was determined. The applied potential of  $+3.00 \text{ V/SCE}$  corresponded to the applied current density of  $11.0 \text{ A}\cdot\text{m}^{-2}$ , and the potential of  $+4.00 \text{ V/SCE}$  corresponded to  $31.0 \text{ A}\cdot\text{m}^{-2}$ . Under the applied potential of  $+3.00 \text{ V/SCE}$ , the electrooxidation was under charge transfer control ( $i < i_{\text{lim}}$ ), and partial degradation and no mineralization of DOX occurred (see Table 2). Under these experimental conditions, OER just started (according to Figure 4), but the required high concentrations of hydroxyl radicals were not achieved to obtain DOX mineralization. However, the highest rate of DOX electrochemical partial degradation via electrooxidation of the dioxyderivative substituents—which was indicated by color removal—was reached. The methoxy substituent and the quinonoid structures were also degraded, without the opening of the aromatic rings.

**Table 2.** Electrochemical efficiency (E) of DOX degradation and mineralization.

Supporting Electrolyte	E/V	Conc. DOX(mg/L)	Time (h)	E <sub>A486</sub> (mg/C·cm <sup>2</sup> )	E <sub>A290</sub> (mg/C·cm <sup>2</sup> )	E <sub>A253</sub> (mg/C·cm <sup>2</sup> )	E <sub>A232</sub> (mg/C·cm <sup>2</sup> )	E <sub>TOC</sub> (mg/C·cm <sup>2</sup> )
0.1 M Na <sub>2</sub> SO <sub>4</sub>	3	2.5	2	5.20	-	2.08	2.08	-
	4	2.5	0.5	0.226	-	0.339	0.339	-
		2.5	1	2.20	0.622	0.962	0.566	0.050
		2.5	2	0.929	0.208	0.388	0.277	0.017
0.05 M Na <sub>2</sub> SO <sub>4</sub> + 0.05 M NaCl	4	2.5	0.5	4.14	2.35	2.35	2.46	0.147
		2.5	1	3.11	1.27	1.58	1.48	0.065
		2.5	2	2.19	0.816	1.19	1.02	0.032
		5	2	2.75	1.22	1.63	1.53	0.032
		10	2	3.26	0.919	1.73	1.83	0.032

-no degradation occurred.

Under the applied potential value of +4.00 V/SCE, the electrooxidation was under mass transfer control ( $i > i_{lim}$ ), and both degradation and mineralization of DOX occurred (see Table 2). Even if the degradation and mineralization degrees ( $\eta$ , %) were higher under the potential of +4.00 V/SCE and increased with the electrooxidation time, the electrochemical degradation degree ( $E$ , mg/C·cm<sup>2</sup>) that considered the electrical charge consumption decreased during the electrolysis time, because a main component of the electrical charge was consumed inside reactions that occurred besides DOX degradation. No mineralization was achieved by electrooxidation at +3.00 V/SCE in the first 30 min of electrolysis operated at +4.00 V/SCE without chloride species. The presence of chloride favored both electrochemical degradation and mineralization, because of Cl<sub>2</sub> generation that contributed to the degradation of DOX.

The effect of DOX concentration on the electrochemical degradation and mineralization degrees in the presence of chloride is also presented in Table 2. It can be noticed that the electrochemical degradation degree was higher as DOX concentration increased, which proved that the DOX electrooxidation process was controlled by mass transport. At DOX concentrations ranging from 2.5 to 10 mg·L<sup>-1</sup>, similar values of the electrochemical mineralization degree were achieved, indicating that the partial degradation of DOX was improved while the mineralization process was not favored.

For a more accurate assessment of the efficacy of the mineralization process, taking into account energy consumption, the chemical oxygen demand (COD) at the initial concentration of 2.5 mg·L<sup>-1</sup> DOX and after electrolysis operated at +4.00 V/SCE in both supporting electrolytes was analyzed. Based on this, the average current efficiency (ACE) was determined according to Equation (12) [42]:

$$ACE = [COD_i - COD_f] \cdot F \cdot \frac{V}{8} \cdot I \cdot t \quad (12)$$

where  $COD_i$  and  $COD_f$  are the initial and the final COD (in gO<sub>2</sub>·dm<sup>-3</sup>);  $I$  is the current intensity (A),  $F$  is the Faraday constant (96,487 C·mol<sup>-1</sup>),  $t$  is the time (s),  $V$  is the volume of the electrolyte (dm<sup>3</sup>), and 8 is a dimensional factor for unit consistence (32 gO<sub>2</sub>·mol<sup>-1</sup>O<sub>2</sub>/4 mol e<sup>-</sup>·mol<sup>-1</sup>O<sub>2</sub>).

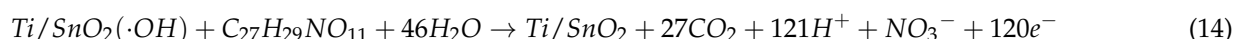
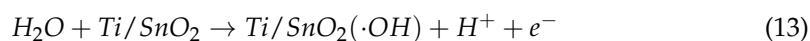
The results are presented in Table 3. It can be noticed that a better average current efficiency was achieved in the presence of chloride, which showed that half of the consumed electrical charge was used for DOX mineralization in comparison with about 19% in 0.1 M Na<sub>2</sub>SO<sub>4</sub>, in which most of the consumed energy was wasted via side reactions occurring to the detriment of DOX mineralization.

**Table 3.** Current efficiency and kinetics aspects determined for the electrolysis of 2.5 mg·L<sup>-1</sup> DOX operated at +4.00 V/SCE.

Supporting Electrolyte	ACE	Kinetics Aspects		
		Degradation/Mineralization	k [min <sup>-1</sup> ]	k' [C <sup>-1</sup> ]
0.1 M Na <sub>2</sub> SO <sub>4</sub>	0.19	A <sub>486</sub>	0.0118	0.194
		A <sub>290</sub>	0.0016	0.025
		A <sub>253</sub>	0.0028	0.051
		A <sub>232</sub>	0.0021	0.035
		TOC	0.0005	0.009
0.05 M Na <sub>2</sub> SO <sub>4</sub> + 0.05 M NaCl	0.50	A <sub>486</sub>	0.0168	0.282
		A <sub>290</sub>	0.0017	0.064
		A <sub>253</sub>	0.0040	0.169
		A <sub>232</sub>	0.0029	0.111
		TOC	0.0015	0.027

In general, the assessment of the kinetics aspects of electrooxidation processes considers a pseudo first-order kinetic model to describe the dependence of the electrochemical reaction rates on the concentration of organic pollutants, expressed as  $\ln(C_0/C_t) = k(t)$ . The rate constant can also be expressed as a function of the electrical charge that is consumed during the electrooxidation process based on  $\ln(C_0/C_t) = k'(C)$ , in which C represents the electrical charge passed during the electrochemical oxidation of DOX [43]. The kinetics results confirmed that the presence of chloride in the supporting electrolyte composition improved DOX degradation, which is in accordance with the literature [7]. The mineralization process of DOX was also improved from the technical-economic point of view, considering the energy consumption by chlorine electrochemically generated at the Ti/SnO<sub>2</sub> electrode in the presence of chloride in accordance with reactions (6, 7).

From the kinetics point of view, the results related to the rate constants for DOX degradation are similar to those reported in the literature using a BDD electrode for DOX and other cytostatics [6,7]. However, the mineralization current efficiency achieved with the 3-D Ti/SnO<sub>2</sub> was better in comparison with that reported for the BDD electrode used for the mineralization of other cytostatics [6] and of tetracycline, which belongs to similar class of anthracycline compounds [8]. Based on the electrochemical characterization results of Ti/SnO<sub>2</sub> and its testing in DOX degradation and mineralization corroborated by the literature data [44,45], the degradation and mineralization process can be governed by electron transfer at the electrode surface–aqueous supporting electrolyte solution interface and/or by diffusion into the bulk solution of the hydroxyl radicals generated and adsorbed on the electrode surface in agreement with reactions (13–14) [7,46–48].



The above-presented results support the advanced degradation and mineralization pathway presented in Scheme 1.



presented findings. In conclusion, this study successfully developed a new and effective anodic material that can be applied for the electrochemical conversion and mineralization of doxorubicin, a frequently used cytostatic and an emerging water pollutant from.

**Author Contributions:** Conceptualization, F.M.; methodology, F.M. and C.O.; investigation, C.B., M.I.P. and A.B.; resources, F.M., A.B. and C.L.; writing—original draft preparation, C.O., C.L. and F.M.; writing—review and editing, F.M. and C.O. All authors have read and agreed to the published version of the manuscript.

**Funding:** This research received no external funding.

**Acknowledgments:** This work was supported partially by a grant from the Romanian Ministry of Education and Research, CNCS—UEFISCDI, project code project code PN-III-P2-2.1-PED-2019-4492, contract number 441PED/2020 (3DSAPECYT), partially by project number project code PN-III-P2-2.1-PTE-2019-0394 with contract number 54 PTE/2020; “Intelligent system for water quality monitoring”.

**Conflicts of Interest:** The authors declare no conflict of interest.

## References

1. Barişçia, S.; Turkaya, O.; Ulusoya, E.; Şeker, M.G.; Yüksela, E.; Dimogloa, A. Electro-oxidation of cytostatic drugs: Experimental and theoretical identification of by-products and evaluation of ecotoxicological effects. *Chem. Eng. J.* **2018**, *334*, 1820–1827. [[CrossRef](#)]
2. Pieczynska, A.; Ochoa-Chavez, S.A.; Wilczewska, P.; Bielicka-Giełdon, A.; Siedlecka, E.M. Insights into mechanisms of electrochemical drug degradation in their mixtures in the split-flow reactor. *Molecules* **2019**, *24*, 4356. [[CrossRef](#)] [[PubMed](#)]
3. Jureczko, M.; Kalka, J. Cytostatic pharmaceuticals as water contaminants. *Eur. J. Pharmacol.* **2020**, *866*, 172816. [[CrossRef](#)] [[PubMed](#)]
4. Rybczynska-Tkaczyk, K.; Kornilowicz-Kowalska, T.; Szychowski, K.A. Possibility to biotransform anthracyclines by peroxidases produced by bjerkandera CCBAS 930 with reduction of geno- and cytotoxicity and pro-oxidative activity. *Molecules* **2021**, *26*, 462. [[CrossRef](#)] [[PubMed](#)]
5. Bouma, J.; Beijnen, J.H.; Bult, A.; Underberg, W.J.M. Anthracycline antitumour agents. *Pharm. Weekbl. Sci. Ed.* **1986**, *8*, 109–133. [[CrossRef](#)]
6. Siedlecka, E.M.; Ofiarska, A.; Borzyszkowska, A.F.; Bialk-Bielinska, A.; Stepnowski, P.; Pieczynska, A. Cytostatic drug removal using electrochemical oxidation with BDD electrode: Degradation pathway and toxicity. *Water Res.* **2018**, *144*, 235–245. [[CrossRef](#)]
7. Garcia, L.F.; Gonçalves Moreno, E.K.; Barroso Brito, L.; Rodrigues de Oliveira, G.A.; Linares, J.J.; de Souza Gil, E. Effective degradation of the antineoplastic doxorubicin by electrochemical oxidation on boron doped diamond. *J. Electroanal. Chem.* **2020**, *870*, 114252. [[CrossRef](#)]
8. Vasilie, S.; Manea, F.; Baciu, A.; Pop, A. Dual use of boron-doped diamond electrode in antibiotics-containing water treatment and process control. *Process. Saf. Environ. Prot.* **2018**, *117*, 446–453. [[CrossRef](#)]
9. Ching-Ju, M.C.; Tsan-Yao, C.; Menshan, L.; Chiung-Fen, C.; Yu-Ting, L.; Yu-Tsun, K. Effective anodic oxidation of naproxen by platinum nanoparticles coated FTO glass. *J. Hazard. Mater.* **2014**, *277*, 110–119.
10. Bampos, G.; Petala, A.; Frontistis, Z. Recent trends in pharmaceuticals removal from water using electrochemical oxidation processes. *Environments* **2021**, *8*, 85. [[CrossRef](#)]
11. Da Silva, S.W.; Welter, J.B.; Albornoz, L.L.; ArenhartHeberle, A.N.; Zoppas Ferreira, J.; Moura Bernardes, A. Advanced electrochemical oxidation processes in the treatment of pharmaceutical containing water and wastewater: A review. *Curr. Pollut. Rep.* **2021**, *7*, 146–159. [[CrossRef](#)]
12. Moreno, E.K.G.; Garcia, L.F.; Lobón, G.S.; Brito, L.B.; Oliveira, G.A.R.; Luque, R.; de Souza Gil, E. Ecotoxicological assessment and electrochemical remediation of doxorubicin. *Ecotoxicol. Environ. Saf.* **2019**, *179*, 143–150. [[CrossRef](#)] [[PubMed](#)]
13. Shestakova, M.; Sillanpää, M. Electrode materials used for electrochemical oxidation of organic compounds in wastewater. *Rev. Environ. Sci. Biotechnol.* **2017**, *16*, 223–238. [[CrossRef](#)]
14. Sirés, I.; Brillas, E.; Oturan, M.A.; Rodrigo, M.A.; Panizza, M. Electrochemical advanced oxidation processes: Today and tomorrow. A review. *Environ. Sci. Pollut. Res.* **2014**, *21*, 8336–8367. [[CrossRef](#)] [[PubMed](#)]
15. Sonia, B.D.; Patel, U.D.; Agrawal, A.; Rupareila, J.P. Application of BDD and DSA electrodes for the removal of RB 5 in batch and continuous operation. *J. Water Process. Eng.* **2017**, *17*, 11–21. [[CrossRef](#)]
16. Comninellis, C. Electrocatalysis in the electrochemical conversion/combustion of organic pollutants for waste water treatment. *Electrochim. Acta* **1994**, *39*, 1857–1862. [[CrossRef](#)]
17. Krstić, V.; Pešovski, B. Reviews the research on some dimensionally stable anodes (DSA) based on titanium. *Hydrometallurgy* **2019**, *185*, 71–75. [[CrossRef](#)]
18. Radjenovic, J.; Sedlak, D.L. Challenges and opportunities for electrochemical processes as next-generation technologies for the treatment of contaminated water. *Environ. Sci. Technol.* **2015**, *49*, 11292–11302. [[CrossRef](#)]

19. Seibert, D.; Zorzo, C.F.; Borba, F.H.; de Souza, R.M.; Quesada, H.B.; Bergamasco, R.; Baptista, A.T.; Inticher, J.J. Occurrence, statutory guideline values and removal of contaminants of emerging concern by Electrochemical Advanced Oxidation Processes: A review. *Sci. Total Environ.* **2020**, *748*, 141527. [CrossRef]
20. Zhong, X.; Yang, B.; Zhang, X.; Jia, J.; Yi, G. Effect of calcining temperature and time on the characteristics of Sb-doped SnO<sub>2</sub> nanoparticles synthesized by the sol-gel method. *Particuology* **2012**, *10*, 365–370. [CrossRef]
21. Zhou, C.; Wang, Y.; Chen, J.; Xu, L.; Huang, H.; Niu, J. High-efficiency electrochemical degradation of antiviral drug abacavir using a penetration flux porous Ti/SnO<sub>2</sub>-Sb anode. *Chemosphere* **2019**, *225*, 304–310. [CrossRef] [PubMed]
22. Duan, Y.; Chen, Y.; Wen, Q.; Duan, T. Fabrication of dense spherical and rhombic Ti/Sb-SnO<sub>2</sub> electrodes with enhanced electrochemical activity by colloidal electrodeposition. *J. Electroanal. Chem.* **2016**, *768*, 81–88. [CrossRef]
23. Sun, Y.; Cheng, S.; Mao, Z.; Lin, Z.; Ren, X.; Yu, Z. High electrochemical activity of a Ti/SnO<sub>2</sub>-Sb electrode electrodeposited using deep eutectic solvent. *Chemosphere* **2019**, *239*, 124715. [CrossRef] [PubMed]
24. Scott, J.I.; Martinez-Gazoni, R.F.; Allen, M.W.; Reeves, R.J. Optical and electronic properties of high quality Sb-doped SnO<sub>2</sub> thin films grown by mist chemical vapor deposition. *J. Appl. Phys.* **2019**, *126*. [CrossRef]
25. Sun, Y.; Cheng, S.; Yu, Z.; Li, L.; Li, C.; Yang, J. Elucidating deactivation mechanisms of Pd-doped and un-doped Ti/SnO<sub>2</sub>-Sb electrodes. *J. Alloys Compd.* **2020**, *834*, 155184. [CrossRef]
26. Xu, H.; Zhang, Q.; Yan, W.; Chu, W. A composite Sb-doped SnO<sub>2</sub> electrode based on the TiO<sub>2</sub> nanotubes prepared by hydrothermal synthesis. *Int. J. Electrochem. Sci.* **2011**, *6*, 6639–6652.
27. Yan, B.; Chen, A.; Shao, C.; Zhu, K. Microrod structure and properties of Sb-doped Ti/SnO<sub>2</sub> anodes prepared by magnetron sputtering. *Sci. Bull.* **2015**, *60*, 2135–2139. [CrossRef]
28. Fauzia, V.; Yusnidar, M.N.; Lalasari, L.H.; Subhan, A.; Umar, A.A. High figure of merit transparent conducting Sb-doped SnO<sub>2</sub> thin films prepared via ultrasonic spray pyrolysis. *J. Alloys Compd.* **2017**, *720*, 79–85. [CrossRef]
29. Yao, P. Effects of Sb doping level on the properties of Ti/SnO<sub>2</sub>-Sb electrodes prepared using ultrasonic spray pyrolysis. *Desalination* **2011**, *267*, 170–174. [CrossRef]
30. Liu, H.; Chen, J.; Hu, R.; Yang, X.; Ruan, H. Facile one-pot synthesis of self-assembled 3-D flower-like SnO<sub>2</sub> architectures and their electrochemical properties. *J. Mater. Sci. Mater. Electron.* **2016**, *27*, 3968–3973. [CrossRef]
31. Fan, J.; Guerrero, M.; Carretero-Genevri, A.; Baro, M.D.; Surinach, S.; Pellicer, E.; Sort, J. Evaporation-induced self-assembly synthesis of Ni-doped mesoporous SnO<sub>2</sub> thin films with tunable room temperature magnetic properties. *J. Mater. Chem. C* **2017**, *5*, 5517–5527. [CrossRef]
32. Caliari, P.C.; Pacheco, M.J.; Ciriaco, L.; Lopes, A. Tannery wastewater: Organic load and sulfide removal dynamics by electrochemical oxidation at different anode materials. *Environ. Technol. Innov.* **2019**, *14*, 100345. [CrossRef]
33. Szafraniec, E.; Majzner, K.; Farhane, Z.; Byrne, H.J.; Lukawska, M.; Oszczapowicz, I.; Chlopicki, S.; Baranska, M. Spectroscopic studies of anthracyclines: Structural characterization and in vitro tracking. *Spectrochim. Acta A Mol. Biomol. Spectrosc.* **2016**, *169*, 152–160. [CrossRef] [PubMed]
34. Manet, I.; Manoli, F.; Zambelli, B.; Andreano, G.; Masi, A.; Cellaic, L.; Monti, S. Affinity of the anthracycline antitumor drugs Doxorubicin and Sabarubicin for human telomeric G-quadruplex structures. *Phys. Chem. Chem. Phys.* **2011**, *13*, 540–551. [CrossRef] [PubMed]
35. Fouillaud, M.; Venkatachalam, M.; Girard-Valenciennes, E.; Caro, Y.; Dufossé, L. Anthraquinones and derivatives from marine-derived fungi: Structural diversity and selected biological activities. *Mar. Drugs* **2016**, *14*, 64. [CrossRef] [PubMed]
36. Thomson, R.H. *Naturally Occurring Quinones*, 2nd ed.; Academic Press: Cambridge, MA, USA, 1971; pp. 44–64.
37. NIST Chemistry WebBook, NIST Chemistry WebBook. Available online: <https://webbook.nist.gov/chemistry> (accessed on 11 January 2022).
38. Eaton, A.D.; Clesceri, L.S.; Rice, E.W.; Greenberg, A.E. *Standard Methods for the Examination of Water and Wastewater*, 21st ed.; APHA-AWWA-WEF: Washington, DC, USA, 2005.
39. Ganiyu, S. Electrochemical Advanced Oxidation Processes for Removal of Pharmaceuticals from Water: Performance Studies for Sub-Stoichiometric Titanium Oxide Anode and Hierarchical Layered Double Hydroxide Modified Carbon Felt Cathode. Ph.D. Thesis, UNESCO-IHE, Institute for Water Education, Delft, The Netherlands, 2 December 2016.
40. Panizza, M.; Michaud, P.A.; Cerisola, G.; Comninellis, C. Anodic oxidation of 2-naphthol at boron-doped diamond electrodes. *J. Electroanal. Chem.* **2001**, *507*, 206–214. [CrossRef]
41. Bard, A.J.; Faulkner, L.R. *Electrochemical Methods: Fundamentals and Applications*; Wiley: New York, NY, USA, 1980.
42. Comninellis, C.; Pulgarin, C. Anodic oxidation of phenol for wastewater treatment. *J. Appl. Electrochem.* **1991**, *21*, 703–708. [CrossRef]
43. Ratiu, C.; Manea, F.; Lazau, C.; Grozescu, I.; Radovan, C.; Schoonman, J. Electrochemical oxidation of p-aminophenol from water with boron-doped diamond anodes and assisted photocatalytically by TiO<sub>2</sub>-supported zeolite. *Desalination* **2010**, *260*, 51–56. [CrossRef]
44. Martinez-Huitle, C.A.; Rodrigo, M.A.; Sires, I.; Scialdone, O. Single and coupled electrochemical processes and reactors for the abatement of organic water pollutants: A critical Review. *Chem. Rev.* **2015**, *115*, 13362–13407. [CrossRef]
45. Sanchez-Montes, S.; Perez, J.F.; Saez, C.; Rodrigo, A.M.; Canizares, P.; Aquino, M.J. Assessing the performance of electrochemical oxidation using DSA® and BDD anodes in the presence of UVC light. *Chemosphere* **2020**, *238*, 124575. [CrossRef]

46. Motoclies, S.; Schinteie, B.; Pop, A.; Negrea, S.; Cretu, C.; Szerb, E.I.; Manea, F. Graphene quantum dots and Cu(I) liquid crystal for advanced electrochemical detection of Doxorubicine in aqueous solutions. *Nanomaterials* **2021**, *11*, 2788. [[CrossRef](#)] [[PubMed](#)]
47. Ilyasov, I.R.; Beloborodov, V.L.; Selivanova, I.A.; Terekhov, R.P. ABTS/PP decolorization assay of antioxidant capacity reaction pathways. *Int. J. Mol. Sci.* **2020**, *21*, 1131. [[CrossRef](#)]
48. Reszka, K.J.; Britigan, B.E. Doxorubicin inhibits oxidation of 2,20-azino-bis(3-ethylbenzothiazoline-6-sulfonate) (ABTS) by a lactoperoxidase/H<sub>2</sub>O<sub>2</sub> system by reacting with ABTS-derived radical. *Arch. Biochem. Biophys.* **2007**, *466*, 164–171. [[CrossRef](#)] [[PubMed](#)]